CZ gate error analysis report (I)

Zihan Chen, Siyuan Chen

March 25, 2024

Contents

1 Layout of this report and summary of results

In this work, we study the Rydberg excitations (both two-photon excitation and single-photon excitation) on Rb-87 atoms and analyze the phase-modulated CZ gate protocol (based on two-photon Rydberg excitation) in [EBK+23] under a realistic model of atomic energy levels in the presence of decay errors and thermo fluctuations. This report is sturctured as follows.

In Sec. 2.1, we describe the relevant Rb-87 energy levels and layout the Rydberg excitation pathways for the two-photon excitation as well as for the single-photon excitation. In Sec. 2.2, we estimate the laser power requirement for the 1013nm laser (two-photon excitation) and for the 297nm laser (single-photon excitation). In Sec. 2.3, we specify the error channels used in this work and simulate the ground state $\leftrightarrow$ Rydberg state Rabi oscillations under these errors. We also examine the relation between atomic temperature and T_2^*. In Sec. 3.1, we provide an overview of common benchmarks for gate fidelity. In Sec. 3.2, we analyze the performance of the phase-modulated CZ gate protocol (with two-photon excitation) in [EBK+23] and estimate the infidelity contribution from each source of error. We estimate the regime of the gate parameters for achieving $\sim 99.9\%$ fidelity. In Sec. 4, we present some remarks and an outlook for future work.

2 Rydberg excitation and Rabi oscillations

2.1 Atomic levels and excitation pathways

In this subsection, we discuss the choice of hyperfine levels for an atomic qubit, Rydberg excitation pathways for the two-photon process and for the single-photon process. For Rb-87, due to systematic imperfections such as a small circular-polarized component of the trapping light and its polarization gradient near the focal region, the energy difference between the two hyperfine levels, which we would like to pick as the basis of our qubit, should be magnetically insensitive to achieve longer single qubit coherence time in optical tweezers. [Lev21, TTZ+13] There are three possible choices:

- $\{5S_{1/2}\,|F=1,m_F=0\rangle,\ 5S_{1/2}\,|F=2,m_F=0\rangle\}$. This is used in experimental works by Lukin et al. on demonstrating (high-fidelity) parallel CZ gates. [LKS+19, EBK+23, BEG+23]
- $\{5S_{1/2}\,|F=1,m_F=-1\rangle,\ 5S_{1/2}\,|F=2,m_F=1\rangle\}$. This is used in a theory paper by Lukin et al. on converting leakage errors during a CZ gate operation to Pauli Z errors. [CLK+22]
- $\{5S_{1/2}\,|F=1,m_F=1\rangle,\ 5S_{1/2}\,|F=2,m_F=-1\rangle\}$. This is similar to the previous choice.

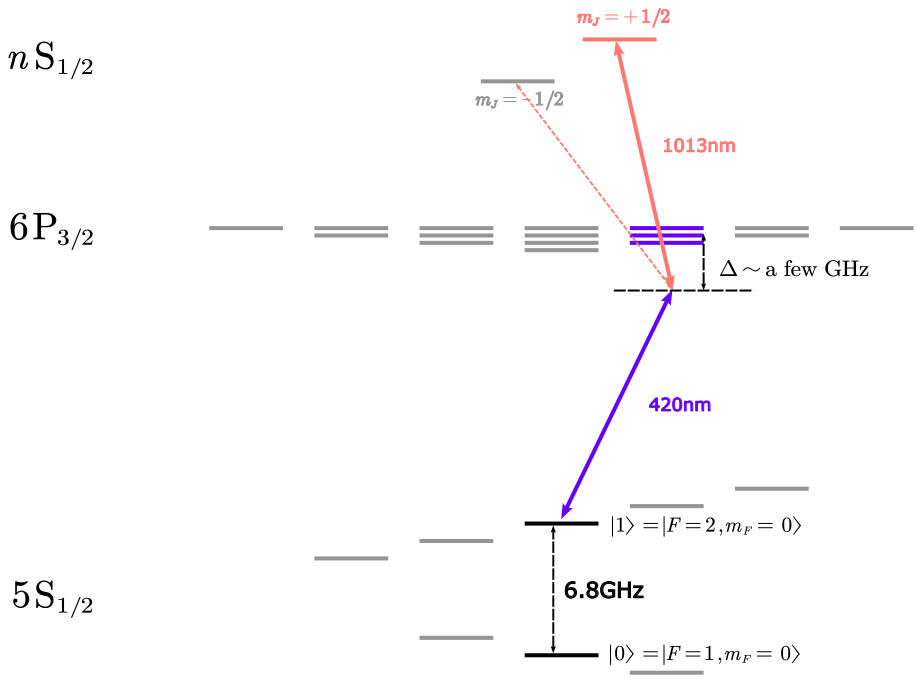

Figure 1: Rb-87 atom levels and two-photon excitation pathways. Three states $6P_{3/2}|F=1,2,3,m_F=1\rangle$ are coupled to $|1\rangle$ by a σ_+ 420nm laser with (red) detuning Δ of a few GHz. A σ_- 1013nm laser is applied so that $|1\rangle$ can be excited to $nS_{1/2}|m_J=\pm1/2\rangle$ via a two-photon process. The effective Rabi frequency of the $|1\rangle\to nS_{1/2}|m_J=-1/2\rangle$ is 1/3 that of the $|1\rangle\to nS_{1/2}|m_J=+1/2\rangle$ transition. A bias magnetic field can be applied to create a splitting between $nS_{1/2}|m_J=\pm1/2\rangle$ to further suppress coupling to $nS_{1/2}|m_J=-1/2\rangle$.[1]

In accordance with [LKS+19, EBK+23], we pick $5S_{1/2}\,|F=1,m_F=0\rangle$ and $5S_{1/2}\,|F=2,m_F=0\rangle$ to be our qubit $|0\rangle$ and $|1\rangle$ states respectively (Fig. 1). For a two-photon excitation to a Rydberg state, we

[1] At low atomic levels, HF splitting is significant and under weak magnetic fields $|F,m_F\rangle$ is a good eigenstate. However, for Rydberg states, HF interaction is weak and $|F,m_F\rangle$ is no longer a good eigenstate even under a weak magnetic field. In this case, $|IJ,m_Im_J\rangle$ is a good eigenstate.

use a σ_+ 420nm laser to couple $|1\rangle$ to $6P_{3/2}$ states with (red) detuning Δ of a few GHz, and a σ_- 1013nm laser to further excite to the $nS_{1/2}$ Rydberg states. We discuss the excitation pathways in the following.

By a σ_+ excitation, $|1\rangle$ can be excited to $6P_{3/2}|F = 0, 1, 2, m_F = 1\rangle$ states which then can be excited to $nS_{1/2}|m_J = +1/2, m_I = -1/2\rangle$ and $nS_{1/2}|m_J = -1/2, m_I = 1/2\rangle$ by a σ_- excitation. In [LKS+19, EBK+23], a bias magnetic field of $8.5G$ is applied perpendicular to the trapping laser direction to create a $\sim$ 24MHz splitting between $nS_{1/2}|m_J = \pm 1/2\rangle$ and thereby preferentially coupling $|1\rangle$ to $nS|m_J = +1/2\rangle$. The unwanted coupling to $nS|m_J = -1/2\rangle$ is further suppressed by the difference of effective Rabi frequencies of the two Rydberg excitations, i.e., the effective Rabi frequency of the $|1\rangle \to nS|m_J = -1/2\rangle$ transition is $1/3$ that of the $|1\rangle \to nS|m_J = 1/2\rangle$ transition.

As for single-photon excitations (driven by a 297nm laser), a σ_+ excitation can couple $|1\rangle$ to $nP_{1/2}|m_J = 1/2\rangle$ and $nP_{3/2}|m_J = 1/2, 3/2\rangle$ while a σ_- excitation can couple $|1\rangle$ to $nP_{1/2}|m_J = -1/2\rangle$ and $nP_{3/2}|m_J = -1/2, -3/2\rangle$. Fortunately, for $n \in (50, 80)$, the energy splitting between $nP_{3/2}$ and $nP_{1/2}$ is about a few hundred MHz (Fig. 9(a) in Appendix. A). Thus coupling to $nP_{3/2}$ can be heavily suppressed.

2.2 Laser power requirement

In this section, we quantitatively analyze laser power requirement for Rydberg excitations. As in [EBK+23, BEG+23], the Rydberg lasers propagate longitudinally in Fig. 2 and are top-hat-shaped. The width, height

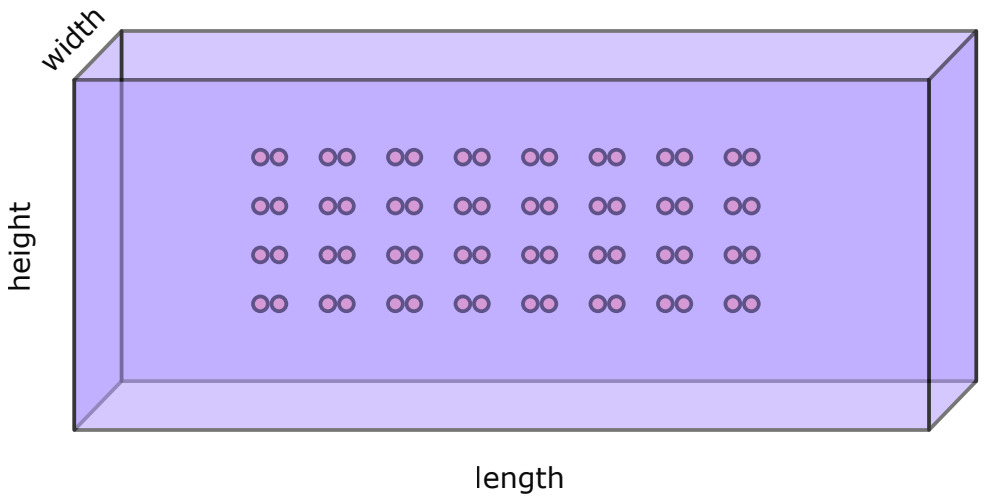

Figure 2: Rydberg top-hat laser beams.

and length of the top-hat region is chosen to be $10\mu m$, $35\mu m$ and $250\mu m$ respectively as in [BEG+23]. With this, we can sustain $\sim$ 80 CZ gate sites (for $\sim$ 160 qubits) at a time in the top-hat region since each CZ gate site is required to be at least $10\mu m$ away from other CZ gate sites. [EBK+23, BEG+23] Under these top-hat parameters, we evaluate the Rabi frequency Ω_{1013} of the $6\,\mathrm{P}_{3/2} \leftrightarrow n\,\mathrm{S}_{1/2}$ transition driven by a 1W 1013nm laser for $n \in [40, 100)$ and observe Ω_{1013} to be about 500MHz at $n = 53$ (Fig. 3). (Notice that Ω_{1013} is set to be 303MHz in [EBK+23].) We make the following observations about the scaling of the 1013nm laser power with the number of CZ gate sites and with the effective Rabi frequency.

- If we keep the length of the top-hat region fixed, then the number of available CZ gate sites grows linearly with the height and thus grows linearly with the 1013nm laser power.
- If the mid-state detuning is fixed, the effective Rabi frequency Ω_{eff} grows linearly with the 1013nm laser power. (Ω_{420} can always easily keep up with Ω_{1013}.)

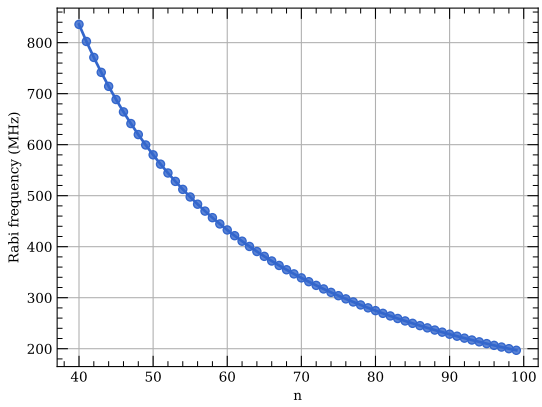

a 1013nm: $6\,\mathrm{P}_{3/2} \leftrightarrow n\,\mathrm{S}_{1/2}$

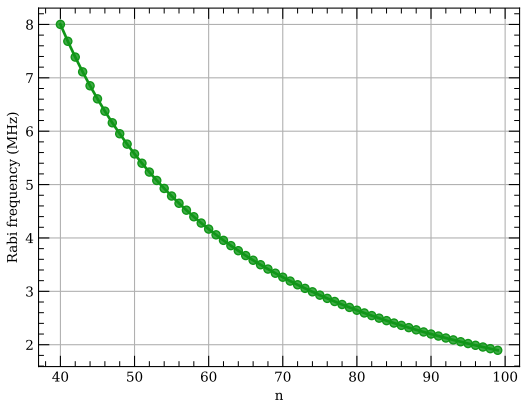

b 297nm: $|1\rangle \leftrightarrow n\,\mathrm{P}_{1/2}$

Figure 3: Rabi frequencies for different levels of Rydberg states under the same laser power. In accordance with [EBK+23, BEG+23], the width and height of the top-hat are $10\mu m$ and $35\mu m$ respectively. **a**, Rabi frequency Ω_{1013} of the $6\,\mathrm{P}_{3/2} \leftrightarrow n\,\mathrm{S}_{1/2}$ transition under a 1W 1013nm laser. **b**, Rabi frequency Ω_{297} of the $|1\rangle \leftrightarrow n\,\mathrm{P}_{1/2}$ transition under a 30mW 297nm laser.

Thus, we expect that 100W power for the 1013nm laser is at least sufficent for realizing $2 \sim 3$k high fidelity ($\sim 99.9\%$) CZ gate sites.

As for the single-photon excitation protocol, we observe, under the same top-hat parameters, when the (σ_- or σ_+) 297nm laser power is 30mW, the Rabi frequency of the $|1\rangle \leftrightarrow nP_{1/2}$ transition is about 5MHz at $n = 53$ (Fig.). (Notice that the effective Rabi frequency Ω_{eff} of $|1\rangle \leftrightarrow 53S_{1/2}$ is 4.6MHz in [EBK+23].) Different from the two-photon excitation protocol, the required 297nm laser power grows quadratically with the ground-Rydberg Rabi frequency.

2.3 Simulation of Rabi oscillations under realistic error channels

In this section, we simulate the Rabi oscillation driven by the two-photon process under the following noise channels with parameters taken from [EBK+23]: (we also present parameters calculated via ARC [ŠPAW17] and address them with *)

- Mid-state scattering. Lifetime of $6\,\mathrm{P}_{3/2}\,|F = 1, 2, 3, m_F = 1\rangle$ is set to be 110ns (118-129ns*). The energy gap between $6\,\mathrm{P}_{3/2}\,|F = 1, m_F = 1\rangle$ and $6\,\mathrm{P}_{3/2}\,|F = 2, m_F = 1\rangle$ is 51MHz (51.4MHz*); the energy gap between $6\,\mathrm{P}_{3/2}\,|F = 2, m_F = 1\rangle$ and $6\,\mathrm{P}_{3/2}\,|F = 3, m_F = 1\rangle$ is 87MHz (86.9MHz*). Moreover, these three hyperfine states share the same $g_F \simeq 2/3$ factor and their energy differences are immune to the bias magnetic field.

- Rydberg decay. Lifetime of $53\,\mathrm{S}_{1/2}$ is set to be 88μs (73μs* at 300K; RD life time: 155μs*, BBR life time: 137μs*).

- Excitation to the unwanted Rydberg state.

- Finite temperature. Rydberg states suffer from random energy shifts due to various imperfections such as the Doppler effect and laser fluctuations. The atomic temperature (or equvalently T_2^*) is a parameter to describe energy shifts with Gaussian distribution. In our simulation, atomic temperature (for a free particle) is set to be 30μK. In this case, random energy shift has Gaussian distribution with standard error $2\pi \times 74.7$kHz. In [EBK+23] by Lukin et al., the measured T_2^* is 3μs, which is

worse than their previous result $T_2^* = 4.5\mu s$ in [LKO+18]. A likely reason for this is that they use higher laser power for larger Rabi frequencies in [EBK+23] and thus suffer from larger laser fluctuations. We numerically examined the relation between atomic temperature and T_2^* and estimate the atomic temperature to be 30μK for $T_2^* = 3\mu s$ (Fig 4).

We choose Ω_{420} to be $2\pi \times 237$MHz (as in [EBK+23]) and Ω_{1013} to be $2\pi \times 275$MHz and simulate the Rabi oscillation between $|1\rangle$ and $53\,S_{1/2}\,|m_J = 1/2\rangle$ under the error channels described above. We obtain a Rabi coherence time $T_1 = 118.86\mu s$, which is the combined result of the Rydberg decay with time scale $176.48\mu s$ and the mid-state scattering with time scale $323.74\mu s$ (Fig. 5). Finite temperature fluctuations are not observed to influence the Rabi oscillations in a significant way.

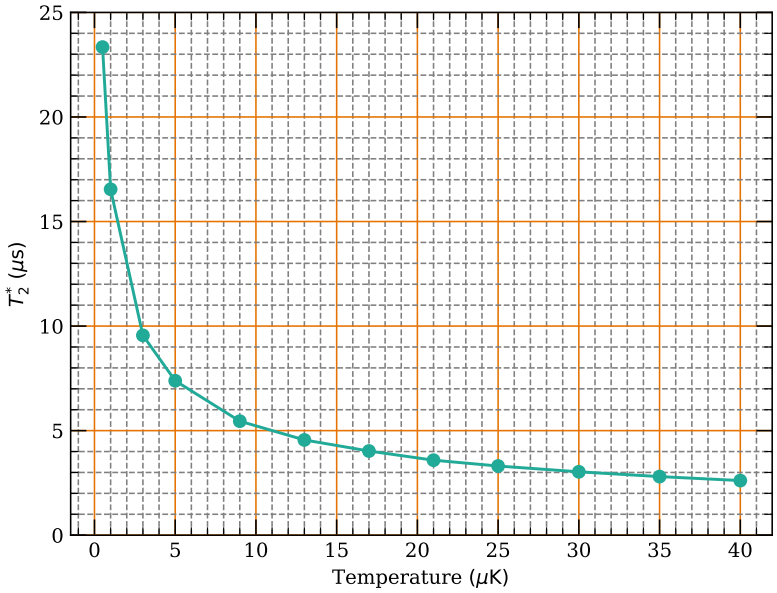

Figure 4: Relation between atomic temperature and T_2^*. At each atomic temperature, T_2^* is obtained via a Ramsey experiment. [LKO+18]

3 Analysis of the CZ gate protocol

3.1 Definition of gate fidelity

To fix the notation throughout this section, we denote the large Hilbert space which encapsulates all relevant states throughout the CZ protocal as $\mathcal{H}$ and the small Hilbert space spanned by $\{|00\rangle, |01\rangle, |10\rangle, |11\rangle\}$ as $\mathcal{H}_{\text{ideal}}$. The ideal CZ gate $U_{\text{ideal}} : \mathcal{H}_{\text{ideal}} \to \mathcal{H}_{\text{ideal}}$ that we wish to implement is simply

$$U_{\text{ideal}} = \text{diag}(0, e^{i\phi_1}, e^{i\phi_1}, e^{i\phi_2}) \tag{1}$$

where $\phi_2 - 2\phi_1 \equiv \pi \mod 2\pi$. The actuall CZ protocol under all possible experimental imperfections and noise would result in a CPTP map $\Lambda : \mathcal{B}(\mathcal{H}) \to \mathcal{B}(\mathcal{H})$. We summarize three benchmarks for gate fidelity in Def. 3.1.

Definition 3.1. [Average gate fidelity, worst case fidelity and Bell state fidelity] The average gate fidelity of Λ inspired by the output state fidelity is defined as

$$\mathcal{F}_{\text{avg}} := \int_{\mathcal{H}_{\text{ideal}}} d\mu_\psi \langle\psi|U_{\text{ideal}}^\dagger \Lambda(|\psi\rangle\langle\psi|) U_{\text{ideal}}|\psi\rangle, \tag{2}$$

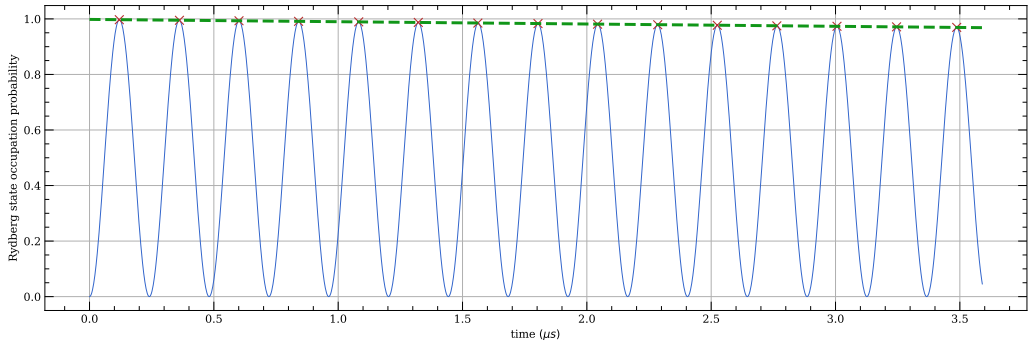

a

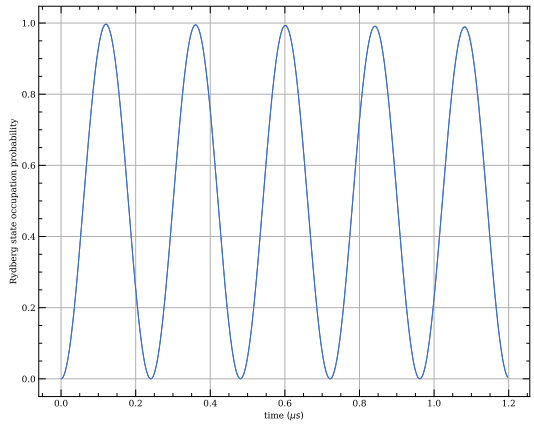

b

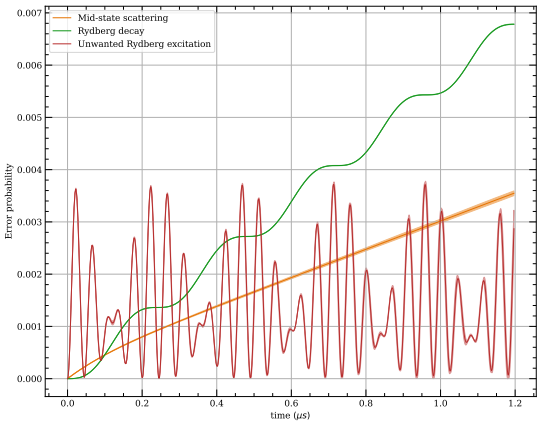

c

Figure 5: Rabi oscillations at 30μK. Shaded areas are used to denote standard deviation. **a**, Rabi oscillation with $\Omega_{420} = 2\pi \times 237$MHz and $\Omega_{1013} = 2\pi \times 275$MHz. The Rabi coherence time T_1 is fitted to be 118.86μs. **b**, The first few cycles of Rabi oscillation in **a**. **c**, Decay errors. The time scale of the Rydberg decay is fitted to be 176.48μs and the time scale of the mid-state scattering is fitted to be 323.74μs. The combination of these two decay is consistent with the Rabi T_1 time. The effect of finite temperature is not pronounced here but is significant in a Ramsey experiment (see Fig. 4).

where the integration is with respect to the Haar measure. Similarly, the worst case fidelity is defined as

$$\mathcal{F}_{\text{worst}} := \inf_{|\psi\rangle \in \mathcal{H}_{\text{ideal}}} \langle\psi|U_{\text{ideal}}^{\dagger}\Lambda(|\psi\rangle\langle\psi|)U_{\text{ideal}}|\psi\rangle. \tag{3}$$

Another frequently used benchmark for gate fidelity is the Bell state fidelity defined as

$$\mathcal{F}_{\text{Bell}} := \langle\psi_+|U_{\text{ideal}}^{\dagger}\Lambda(|\psi_+\rangle\langle\psi_+|)U_{\text{ideal}}|\psi_+\rangle, \tag{4}$$

where the input state $|\psi_+\rangle$ is $|+\rangle|+\rangle$.

The average gate fidelity and worst case fidelity can be naively obtained by sampling over Haar random two-qubit states as input. However, this method is computationally costly and is especially unsuitable when we want to optimize gate parameters based on the gate fidelity. Fortunately, for $\mathcal{F}_{\text{avg}}$, we have an explicit expression. Based on Thm. 3.1, we obtain Prop. 3.1 which makes it possible for us to extract $\mathcal{F}_{\text{avg}}$ efficiently using 16 special input states. (See also [JP22] for a weaker form of Prop. 3.1.) However, $\mathcal{F}_{\text{Bell}}$ is still the most efficient benchmark since it only requires simulation on a single input state. Moreover, we empirically observe in our calculations that the Bell state fidelity is usually slightly smaller than the average gate fidelity. Thus in this work, we use $\mathcal{F}_{\text{Bell}}$ as an objective function to optimize the gate parameters and also as the final benchmark for gate fidelity.

Theorem 3.1. [PMM07] For any linear operator M on $\mathcal{H}_{\text{ideal}}$,

$$\int_{\mathcal{H}_{\text{ideal}}} d\mu_\psi |\langle\psi|M|\psi\rangle|^2 = \frac{1}{d(d+1)}\left[\text{Tr}(MM^\dagger) + |\,\text{Tr}(M)|^2\right], \tag{5}$$

where $d := \dim \mathcal{H}_{\text{ideal}} = 4$.

Proposition 3.1. The average gate fidelity of our CZ operation Λ has the following explicit expression.

$$\mathcal{F}_{\text{avg}} = \frac{1}{20}\left[\sum_i \langle i|\Lambda(\mathbb{1}_{\mathcal{H}_{\text{ideal}}})|i\rangle + \sum_{i,j} e^{-i(\phi_i-\phi_j)}\langle i|\Lambda(|i\rangle\langle j|)|j\rangle\right], \tag{6}$$

where the summation for each index is over $\{00, 01, 10, 11\}$ with $\phi_{00} = 0$, $\phi_{01} = \phi_{10} = \phi_1$ and $\phi_{11} = \phi_2$.

3.2 Error analysis of the phase modulation protocol

In this section, we focus on the phase modulation protocol used in [EBK+23]. This protocol works as follows. The 1013nm laser has its amplitude and phase fixed throughout the gate implementation while the 420nm laser is pulsed on and then maintained at a fixed Rabi frequency with a smoothly modulated phase

$$\phi(t) = A\cos(\omega t + \varphi_0) + \delta t, \tag{7}$$

before being turned off at a specific time. We assume, at the beginning/end of the protocol, a finite rise/fall time of 20ns during which the 420nm laser pulse has a Blackman intensity profile. [EBK+23] The coefficients A, ω, φ, δ in Eq. 7 and the total gate time are numerically optimized to reach maximum Bell state fidelity $\mathcal{F}_{\text{Bell}}$. We provide a heuristic argument on why this protocal may realize a CZ gate in the following. First, notice that this protocol does nothing to an atom on state $|0\rangle$ and does not allow (at least in the ideal setting) transfering $|1\rangle$ to $|0\rangle$. Thus, our only choice is to make each basis state $|00\rangle$, $|01\rangle$, $|10\rangle$ and $|11\rangle$ return to itself after the protocol. In this way, this protocol implements a CPHASE(θ) gate and by tuning the parameters, we may realize a CZ gate.

As in [EBK+23], the Rydberg interaction of $53\,S_{1/2}\,|m_J=1/2\rangle|m_J=1/2\rangle$ at 2μm is taken to be $2\pi\times 450$MHz ($2\pi\times 446$MHz via ARC [ŠPAW17]). As for the influence of the unwanted Rydberg state $53\,S_{1/2}\,|m_J=-1/2\rangle$, the energy shifts of $53\,S_{1/2}\,|m_J=-1/2\rangle|m_J=1/2\rangle$ as well as $53\,S_{1/2}\,|m_J=-1/2\rangle|m_J=-1/2\rangle$ are also roughly $2\pi\times 450$MHz at the same inter-atomic distance. (Actually, there is also a slow tunneling $\sim$ 10MHz between $53\,S_{1/2}\,|m_J=-1/2\rangle|m_J=1/2\rangle$ and $53\,S_{1/2}\,|m_J=1/2\rangle|m_J=-1/2\rangle$. However, this effect does not interfere much with our analysis as the excitation to two-Rydberg states is blockaded.) It seems that the Rydberg interaction contributed by the unwanted Rydberg state is not taken into account (at least not explicitly) in [EBK+23]. We analyze the CZ gate protocol both with and without the Rydberg interaction from the unwanted Rydberg state and mark the latter case with ▲.

Error source	Our analysis	analysis in [EBK+23]
Mid-state scattering	0.0999% / 0.1002%▲	0.103% (bright)/ 0.043% (dark)
Rydberg decay	0.1368% / 0.1322%▲	0.113%
Unwanted Rydberg excitation	0.0429% / <0.0011%▲	0.060% $\sim$ 0.15%
Thermo (30μK/$T_2^*=3\mu$s)	0.1100% / 0.1031%▲	0.134%
(Bell state) fidelity (0μK)	99.720% / 99.767%▲	99.66$\sim$99.75%
(Bell state) fidelity (30μK/$T_2^*=3\mu$s)	99.610% / 99.664%▲	99.53$\sim$99.62%

Table 1: Error source analysis for the phase-modulated CZ gate protocol. According to the sign of the initial phase φ_0, the protocol can be categorized as either bright(+) or dark(−). We use the latter for our analysis. The results, in which the Rydberg interaction from the unwanted Rydberg state is considered, are marked with ▲. The presence of the Rydberg interaction from the unwanted Rydberg state is actually helpful to alleviate the negative impact of the unwanted Rydberg interaction. Other error channels are basically indifferent towards the Rydberg interaction from the unwanted Rydberg state.

Under Rabi frequencies $\Omega_{420}/2\pi=237$MHz, $\Omega_{1013}/2\pi=303$MHz, the mid-state detuning $\Delta/2\pi=7.8$GHz as in [EBK+23] and the same noise channels specified in Sec. 2.3, we obtain an optimized Bell state fidelity of 99.720% (99.767%▲) at 0μK (Tab. 1) and under the same gate parameters, the Bell state fidelity drops to 99.610% (99.664%▲) at 30μK (which we expect corresponds to $T_2^*=3\mu$K in [EBK+23]). At the end of the gate protocol, the contribution from the Rydberg decay (to the final state) is 0.1368% (0.1322%▲), and is 0.0999% (0.1002%▲) from the mid-state scattering; moreover, there is about 0.0429% ($<0.0001\%$▲) of population on the unwanted Rydberg state $53\,S_{1/2}\,|m_J=-1/2\rangle$ (Tab. 1, Fig. 6, Fig. 7▲). These three terms in total contributes about 0.2796% (0.2334%▲) infidelity. Thus, at 0μK, the major error comes from these three sources (the Mid-state scattering and the Rydberg decay▲) and apart from them, the gate protocol manages to bring the final state back to the qubit subspace (residual Rydberg occupation $<0.0001\%$) and deliver the correct (relative) phase shifts. At a finite temperature of 30μK, the above three error sources do not change appreciably (Fig. 6), and the residual Rydberg occupation is still small ($\sim 0.001\%/0.003\%$▲), we thus infer that the effect of a finite temperature is to perturb the single-qubit and/or the two-qubit phase shift and thereby decreasing the Bell state fidelity. We do notice some discrepancies between our analysis and that of the work [EBK+23], however, we are not able to find an explanation for it (Tab.1).

Based on previous analysis, we heuristically argue how to suppress the infidelity to 0.1% in the following. Firstly, the Rydberg decay is proportional to the total gate time and thus is proportional to $1/\Omega_{\text{eff}}$. In this way, by increasing Ω_{eff} by 3 times, we expect the Rydberg decay would be suppressed to about 0.045%. Secondly, the mid-state occupation is proportional to $(\Omega_{420}/\Delta)^2\propto\Omega_{\text{eff}}/\Delta$, which means the

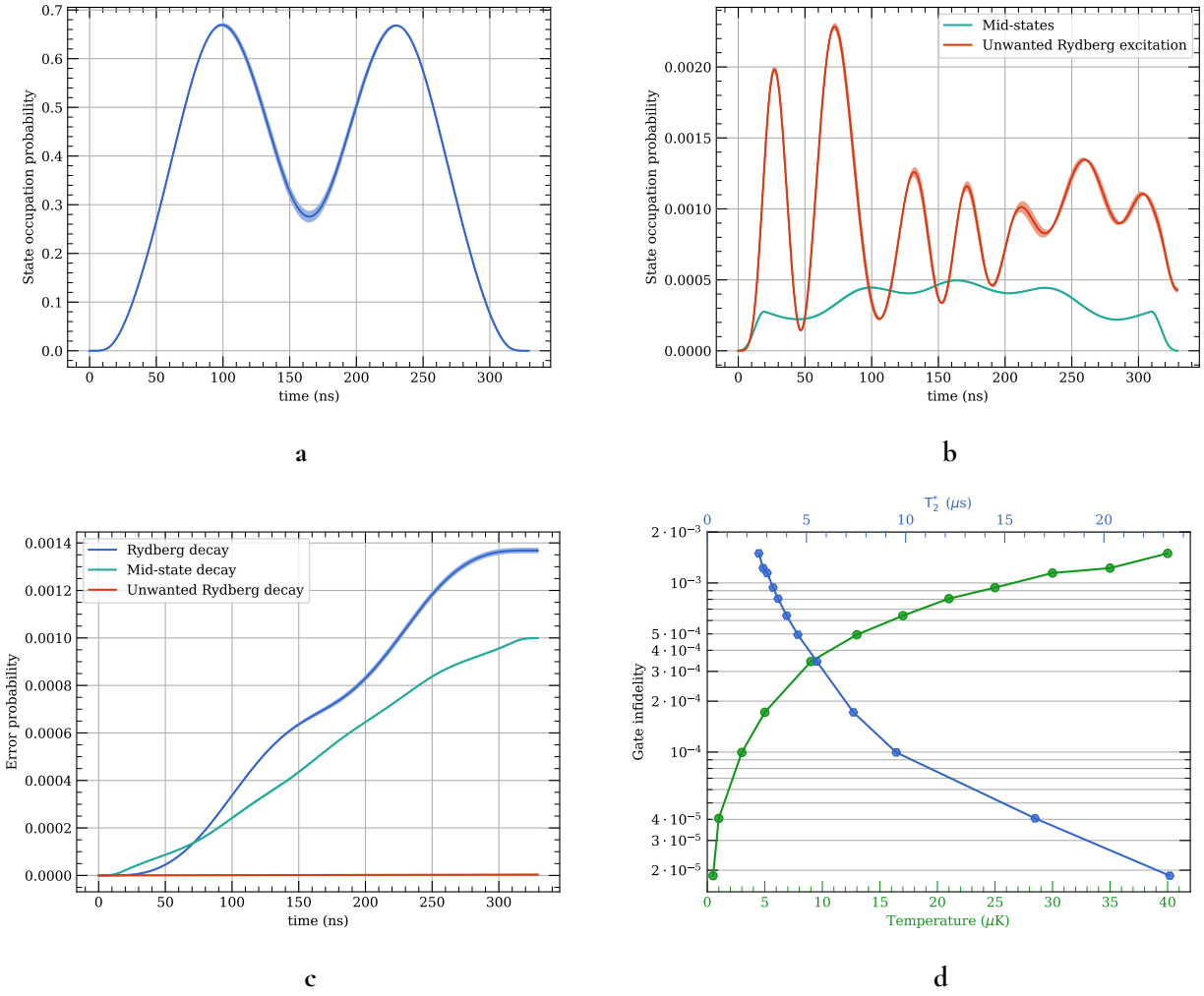

Figure 6: Analysis of phase-modulated CZ gate protocol at 30μK. Rydberg interaction from the unwanted Rydberg state is NOT taken into account. Shaded areas are used to denote standard deviation. **a**, Occupation of the Rydberg state during the protocol. **b**, Occupation of the middle states and the unwanted Rydberg state. **c**, Error probability of three decay channels: Rydberg decay, mid-state scattering and decay from the unwanted Rydberg state. **d**, Thermo contribution to the gate infidelity.

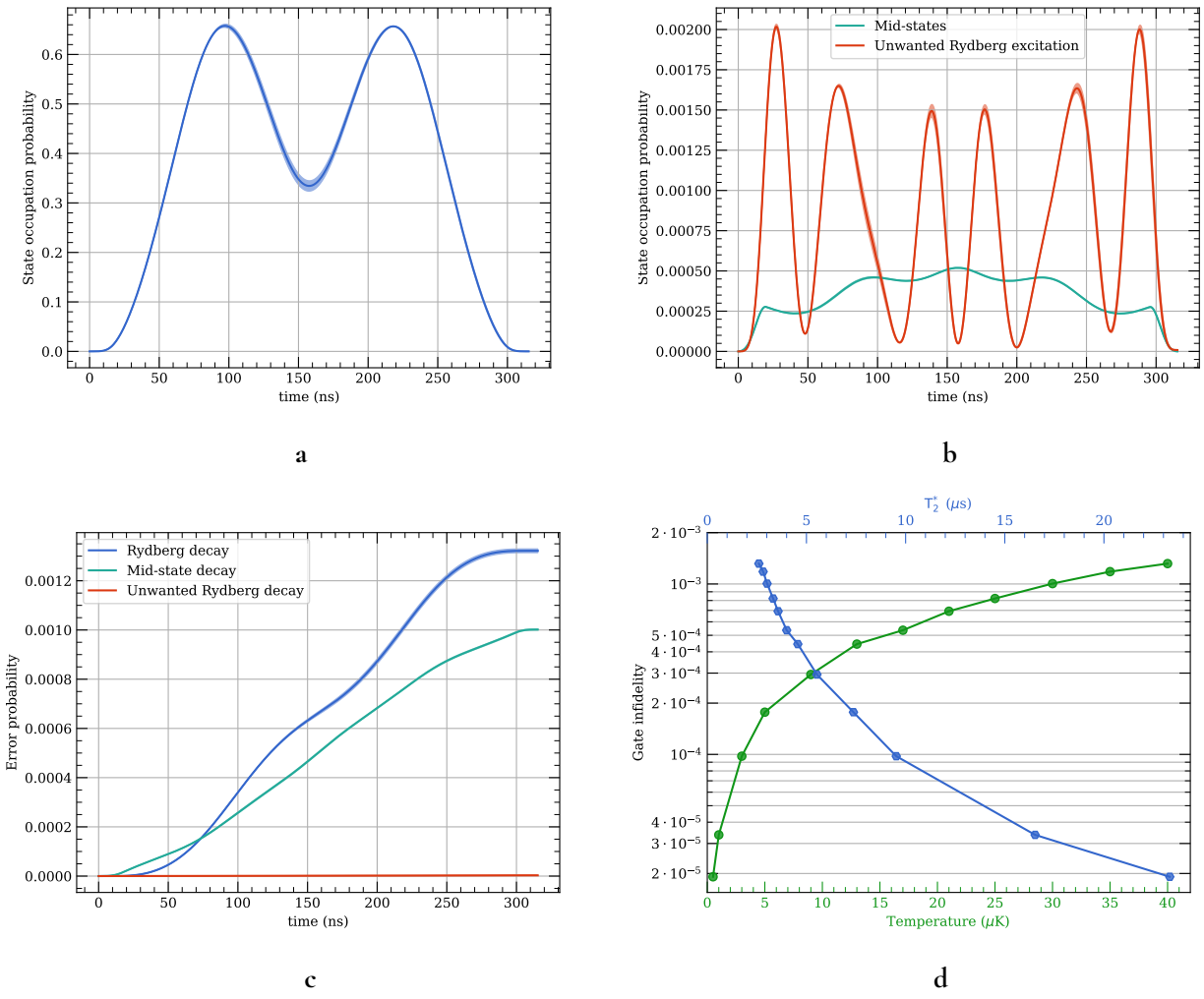

Figure 7: Analysis of phase-modulated CZ gate protocol at 30μK. Rydberg interaction from the unwanted Rydberg state is taken into account. Shaded areas are used to denote standard deviation. **a**, Occupation of the Rydberg state during the protocol. **b**, Occupation of the middle states and the unwanted Rydberg state. Due to the Rydberg interaction introduced by the unwanted Rydberg state, its occupation throughout the CZ protocol is drastically different from Fig. 6b. **c**, Error probability of three decay channels: Rydberg decay, mid-state scattering and decay from the unwanted Rydberg state. **d**, Thermo contribution to the gate infidelity.

mid-state scattering is proportional to $1/\Delta$. Thus, if we use a $2\times$ larger mid-state detuning, we expect the mid-state scattering would decrease to 0.050%. Similarly, the unwanted Rydbert excitation is proportional to $(\Omega_{\text{eff}}/B_z)^2$, where B_z is the bias magnetic field. So, now that Ω_{eff} is $3\times$ higher than before, we need to increase B_z by 6 times so that we expect the infidelity contribution from the unwanted Rydberg excitation would drop to 0.01% ($< 0.0005\%$▲). Lastly, as for the thermo effect, since the Ramsey experiment predicts that the return probability has a Gaussian decay $\propto \exp(-(t/T_2^*)^2)$, we expect the thermo infidelity is proportional to $1/(\Omega_{\text{eff}}T_2^*)^2$. Then, under the new choice of Ω_{eff}, we expect the thermo infidelity drops to 0.012% with the temperature fixed at 30μK. Then, under this new parameter regime, we expect our gate fidelity at 0μK to be 99.89% and our gate fidelity at 30μK to be 99.88%, which is fairly close to a triple-nine fidelity. Our argument above is corroborated by the simulation results (Tab. 2).

Error source	Crude estimation	Numerical result
Mid-state scattering	0.05%	0.0500% / 0.0503%▲
Rydberg decay	0.045%	0.0408% / 0.0406%▲
Unwanted Rydberg excitation	0.01% / <0.0005%▲	0.0001% / <0.0001%▲
Thermo (30μK/$T_2^* = 3\mu$s)	0.012%	0.0108%
(Bell state) fidelity (0μK)	99.89%	99.909%
(Bell state) fidelity (30μK/$T_2^* = 3\mu$s)	99.88%	99.898%

Table 2: Towards a higher CZ gate fidelity with amplified gate parameters. Analysis of gate fidelity under a $3\times$ higher Ω_{eff} (a $\sqrt{6}\times$ higher Ω_{420} and a $\sqrt{6}\times$ higher Ω_{1013}), a $2\times$ higher Δ, a $6\times$ higher bias magnetic field B_z and at the same atomic temperature. The unwanted Rydberg excitation is heavily suppressed here not only because of the higher bias magnetic field but also because of a smoother pulse shape (due to a $3\times$ higher rise time/total gate time ratio). In this case, the presence of the Rydberg interaction from the unwanted Rydberg state seems irrelevant.

4 Final remarks and outlook

In this work, we provide a basic estimation of required Rydberg laser power for implementing medium scale high-fidelity CZ gate sites and a careful error analysis of the phase-modulated CZ gate protocol with two-photon Rydberg excitation [EBK+23]. We only briefly touch upon single-photon excitation in Sec. 2.1- 2.2 and a similar analysis for CZ gate errors is due in future work. While we incorporated all kinds of decay errors and the thermo effect in our analysis of the CZ gate protocol, we still have not yet considered the influence of laser noise (phase noise as well as intensity noise). We intend to investigate its impact on the CZ gate fidelity in a future work. Also, for experimental/theoretical work on fault tolerance, a detailed model of error channels would be very helpful. We estimated the gate infidelity from various errors in this work, we still need to go one step further to obtain the exact CPTP map corresponding to these errors. Due to BBR and decay to other hyperfine ground states, we expect a significant portion of the error to be leakage error which lies beyond the Stabilizer formalism and is especially harmful to performing quantum error correction. There are a few proposals [WKPT22, CLK+22] that convert such dangerous leakage errors to more "benign" Pauli errors, however, a more careful look into the extra errors introduced during the conversion process as well as more resource-efficient designs are still needed.

References

[BEG+23] Dolev Bluvstein, Simon J. Evered, Alexandra A. Geim, Sophie H. Li, Hengyun Zhou, Tom Manovitz, Sepehr Ebadi, Madelyn Cain, Marcin Kalinowski, Dominik Hangleiter, J. Pablo Bonilla Ataides, Nishad Maskara, Iris Cong, Xun Gao, Pedro Sales Rodriguez, Thomas Karolyshyn, Giulia Semeghini, Michael J. Gullans, Markus Greiner, Vladan Vuletić, and Mikhail D. Lukin. Logical quantum processor based on reconfigurable atom arrays. *Nature*, 626(7997):58–65, December 2023. URL: http://dx.doi.org/10.1038/s41586-023-06927-3, doi:10.1038/s41586-023-06927-3.

[CLK+22] Iris Cong, Harry Levine, Alexander Keesling, Dolev Bluvstein, Sheng-Tao Wang, and Mikhail D. Lukin. Hardware-efficient, fault-tolerant quantum computation with rydberg atoms. *Phys. Rev. X*, 12:021049, Jun 2022. URL: https://link.aps.org/doi/10.1103/PhysRevX.12.021049, doi:10.1103/PhysRevX.12.021049.

[EBK+23] Simon J. Evered, Dolev Bluvstein, Marcin Kalinowski, Sepehr Ebadi, Tom Manovitz, Hengyun Zhou, Sophie H. Li, Alexandra A. Geim, Tout T. Wang, Nishad Maskara, Harry Levine, Giulia Semeghini, Markus Greiner, Vladan Vuletić, and Mikhail D. Lukin. High-fidelity parallel entangling gates on a neutral-atom quantum computer. *Nature*, 622(7982):268–272, October 2023. URL: http://dx.doi.org/10.1038/s41586-023-06481-y, doi:10.1038/s41586-023-06481-y.

[JP22] Sven Jandura and Guido Pupillo. Time-optimal two- and three-qubit gates for rydberg atoms. *Quantum*, 6:712, May 2022. URL: http://dx.doi.org/10.22331/q-2022-05-13-712, doi:10.22331/q-2022-05-13-712.

[Lev21] Harry Jay Levine. *Quantum information processing and quantum simulation with programmable Rydberg atom arrays*. PhD thesis, Harvard University, 2021.

[LKO+18] Harry Levine, Alexander Keesling, Ahmed Omran, Hannes Bernien, Sylvain Schwartz, Alexander S. Zibrov, Manuel Endres, Markus Greiner, Vladan Vuletić, and Mikhail D. Lukin. High-fidelity control and entanglement of rydberg-atom qubits. *Phys. Rev. Lett.*, 121:123603, Sep 2018. URL: https://link.aps.org/doi/10.1103/PhysRevLett.121.123603, doi:10.1103/PhysRevLett.121.123603.

[LKS+19] Harry Levine, Alexander Keesling, Giulia Semeghini, Ahmed Omran, Tout T. Wang, Sepehr Ebadi, Hannes Bernien, Markus Greiner, Vladan Vuletić, Hannes Pichler, and Mikhail D. Lukin. Parallel implementation of high-fidelity multiqubit gates with neutral atoms. *Physical Review Letters*, 123(17), October 2019. URL: http://dx.doi.org/10.1103/PhysRevLett.123.170503, doi:10.1103/physrevlett.123.170503.

[PMM07] Line Hjortshøj Pedersen, Niels Martin Møller, and Klaus Mølmer. Fidelity of quantum operations. *Physics Letters A*, 367(1–2):47–51, July 2007. URL: http://dx.doi.org/10.1016/j.physleta.2007.02.069, doi:10.1016/j.physleta.2007.02.069.

[ŠPAW17] N. Šibalić, J.D. Pritchard, C.S. Adams, and K.J. Weatherill. Arc: An open-source library for calculating properties of alkali rydberg atoms. *Computer Physics Communications*, 220:319–331, November 2017. URL: http://dx.doi.org/10.1016/j.cpc.2017.06.015, doi:10.1016/j.cpc.2017.06.015.

[TTZ+13] J. D. Thompson, T. G. Tiecke, A. S. Zibrov, V. Vuletić, and M. D. Lukin. Coherence and raman sideband cooling of a single atom in an optical tweezer. *Physical Review Letters*, 110(13), March 2013. URL: http://dx.doi.org/10.1103/PhysRevLett.110.133001, doi:10.1103/physrevlett.110.133001.

[WKPT22] Yue Wu, Shimon Kolkowitz, Shruti Puri, and Jeff D. Thompson. Erasure conversion for fault-tolerant quantum computing in alkaline earth rydberg atom arrays. *Nature Communications*, 13(1), August 2022. URL: http://dx.doi.org/10.1038/s41467-022-32094-6, doi:10.1038/s41467-022-32094-6.

A Rydberg energy levels

In this section, we present a few quantitative properties of Rydberg energy levels for future reference.

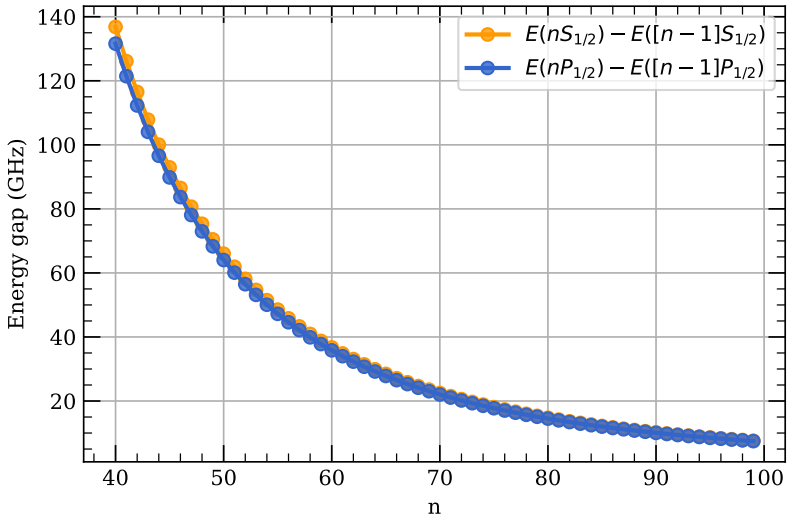

Figure 8: Energy spacing for different n levels of Rydberg states. The corresponding curve for $n\,\mathrm{P}_{3/2}$ states basically overlaps with the curve for $n\,\mathrm{P}_{1/2}$ states and is not shown in the plot.

For $n \sim (50, 70)$, the energy spacing between the $n\,\mathrm{X}$ level and the $(n-1)\,\mathrm{X}$ level, where X can be S or P, is about a few tens of GHz (Fig. 8); the energy splitting between $n\,\mathrm{P}_{1/2}$ and $n\,\mathrm{S}_{1/2}$ is also about a few tens of GHz; the energy splitting between $n\,\mathrm{P}_{3/2}$ and $n\,\mathrm{P}_{1/2}$ is substantially smaller than the previous two and is about a few hundreds of MHz (Fig. 9a-b).

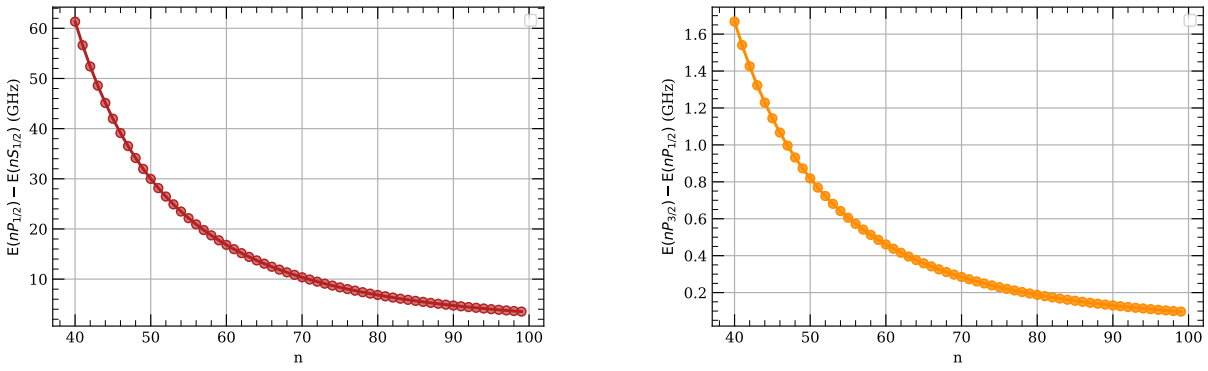

a b

Figure 9: Energy splitting between different L/J levels.